Characterization and Modeling of Reduced-Graphene Oxide Ambipolar Thin-Film Transistors

Nicolò Lago, *Member, IEEE*, Marco Buonomo, Rafael Cintra Hensel, Francesco Sedona, Mauro Sambi, Stefano Casalini, and Andrea Cester, *Senior Member, IEEE*

***Abstract*—The rise of graphene as an innovative electronic material promoted the study and development of new 2-D materials. Among them, reduced graphene oxide (rGO) appears like an easy and cost-effective solution for the fabrication of thin-film transistors (TFTs). To understand the limits and possible application fields of rGO-based TFTs, a proper estimation of the device parameters is of extreme importance. In this work, liquid-gated ambipolar rGO-TFTs are characterized and a description of their working principle is given. Particular attention is paid toward the importance of the transistors' OFF-state conductivity that was modeled as a resistance connected in parallel with the TFT. Thanks to this model, the main transistor parameters were extrapolated from rGO-TFTs with different levels of electrochemical reduction. The extracted parameters allowed understanding that rGO-TFTs have similar holes and electrons mobilities, and the more pronounced p-type behavior of the devices is due to a positive shift in the p-type and n-type threshold voltages.**

***Index Terms*—Ambipolar transistors, liquid-gated transistors, reduced graphene oxide (rGO), thin-film transistors (TFTs).**

I. Introduction

SINCE the pioneering work of Novoselov and Geim, graphene-based electronics became thought-provoking for the entire scientific community [1]. Graphene is a material with remarkable electrical, chemical, mechanical, and optical properties. Among the different fields in which graphene can potentially play a key role, electronics can be stated as one of the major. The reason behind this interest is straightforward: theoretical electron mobility as large as $2{\cdot}10^5$ cm^2 V^{-1} s^{-1} [2]. Although a huge effort has been spent to achieve large-scale production of graphene to satisfy the compelling need of large-area electronics, this technical issue has only been partially solved by chemical vapor deposition and mechanical exfoliation. Within this context, graphene oxide (GO) can play a relevant role because of its water processability and the possibility of tuning its electronic properties via a reduction process, leading to the so-called reduced GO (rGO) [3] that has been successfully implemented for the fabrication of full graphene flexible thin-film transistors (TFTs) [4], as well as liquid-gated rGO-based TFTs [5]. In particular, the latter sets an important technological achievement because the liquid-gated TFT architecture is a fundamental structure in the development of cost-effective bio-chemical transducers (e.g., chemical sensors [6] and neural interfaces [7]) since it allows direct coupling between biological tissues and transistors' active material [8]–[10]. On the other hand, this achievement highlights the importance of proper characterization and modeling of rGO-TFTs to understand fully the working mechanisms of this class of devices.

A common characteristic of rGO-TFTs is a prominent ambipolar behavior that, on the one hand, it proves that field-effect modulation of both electrons and hole is possible, driving researchers' efforts toward the dream of achieving graphene-based complementary electronics exceeding silicon limitations. On the other hand, such ambipolarity comes together with an always-ON behavior, a consequence of the extremely narrow energy bandgap of the rGO active material [11]. This leads to large OFF-currents that severely limit rGO-TFTs' possible applications. So far, the main examples are limited to sensors, which profit from the chemical properties of GO, whose chemical backbone offers several routes of (bio-)chemical functionalization. This approach leads to electronic transducers capable of exploiting devices' high capacitance [12], [13], without really taking advantage of the transistor properties in the implementation of electronic devices and circuits. In fact, the absence of a proper OFF-state prevents the making of low-power consumption digital circuits (in the literature, I_{ON}/I_{OFF}

Manuscript received 17 February 2022; revised 15 April 2022; accepted 18 April 2022. Date of publication 4 May 2022; date of current version 24 May 2022. This work was supported in part by the University of Padua, Department of Information Engineering, under Project PROACTIVE 2018. The work of Rafael Cintra Hensel and Stefano Casalini was supported in part by the University of Padua, Department of Chemical Sciences under Grant P-DiSC#11NExuS_BIRD2020-UNIPD-CARBON-FET and in part by the Italian Ministry of Education, Universities and Research (Nanochemistry for Energy and Health, NExuS, within the National Funding Network termed "Dipartimenti di Eccellenza"). The work of Francesco Sedona and Mauro Sambi was supported by the University of Padova under Grant P-DISC#09BIRD2019-UNIPD SMOW and Grant CPDA154322 AMNES. The review of this article was arranged by Editor Y. Uraoka. *(Corresponding author: Nicolò Lago.)*

Nicolò Lago, Marco Buonomo, and Andrea Cester are with the Department of Information Engineering, University of Padova, 35131 Padova, Italy (e-mail: lagonico@dei.unipd.it).

Rafael Cintra Hensel, Francesco Sedona, Mauro Sambi, and Stefano Casalini are with the Department of Chemical Sciences, University of Padova, 35131 Padova, Italy (e-mail: stefano.casalini@unipd.it).

Color versions of one or more figures in this article are available at https://doi.org/10.1109/TED.2022.3169451.

Digital Object Identifier 10.1109/TED.2022.3169451

This work is licensed under a Creative Commons Attribution 4.0 License. For more information, see https://creativecommons.org/licenses/by/4.0/

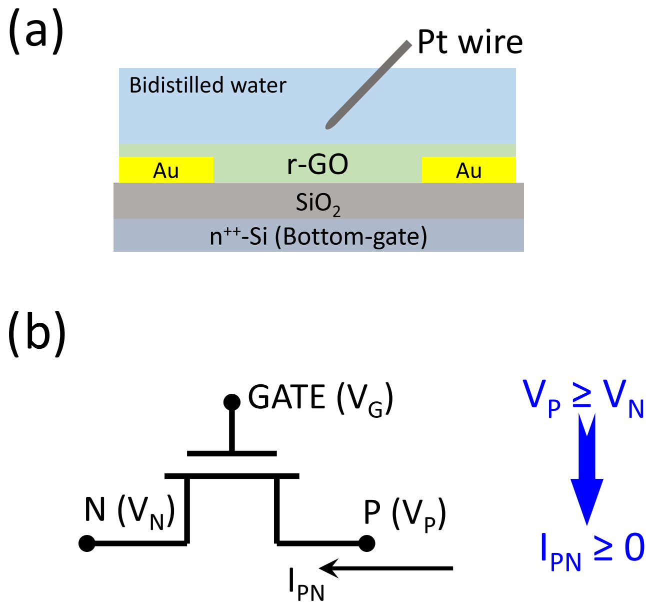

Fig. 1. (a) Sample architecture. (b) Ambipolar TFT convention used in this work.

ratios of just few units are reported [14]); moreover, the low transconductance g_m and the large OFF-current hamper the design of amplifier circuits (values of g_m as large as 0.8 mS have been reported, but they are combined with OFF-currents around 1 mA at 0.1-V drain-to-source bias [15]).

For these reasons, the implementation of graphene derivatives into circuitry is still an open challenge. To understand whether rGO-TFTs can be suitable for a specific application (either digital or analog), it is imperative to grasp the physico-mathematical laws describing the working principle of such a device (namely, current versus voltage characteristics) and to implement a correct extrapolation of the main transistor parameters. Transistors' mobility and threshold voltage are the fundamental information necessary to design any transistor-based electronic circuit, and therefore, their proper estimation is paramount.

In this work, we first provide a generalized description of ambipolar TFTs current versus voltage characteristics valid for disordered materials. Then, we extend this model to rGO-TFTs by including the presence of OFF-state conductivity in parallel to the transistor to consider the large OFF-state current typical of these devices. Finally, this model is implemented to estimate transistor parameters of liquid-gated rGO-TFTs fabricated with different electrochemical reduction levels of the GO layer.

II. Experimental and Devices

A. Devices Fabrication

We fabricated liquid-gated rGO-TFTs onto commercially available silicon substrates with interdigitated gold electrodes [Fig. 1(a)]. The silicon substrates have been purchased from Fondazione Bruno Kessler (Trento, Italy) with the following specifications: 1) n-doped (Sb) silicon with a resistivity of 0.01–0.03 Ω·cm; 2) thermal oxide with a thickness of 200 nm; and 3) Au interdigitated electrodes with a thickness of 100–150 nm and a Cr adhesion layer of 3–5 nm (the TFTs' width W-to-length L ratio is $W/L = 560$). Concerning GO deposition (4 mg·mL^{-1}, monolayer content > 95%, graphene), the substrates were subsequently rinsed with acetone, isopropanol, and bi-distilled water to remove the protective layer. Afterward, the substrates were immersed in a poly(diallylammonium chloride) solution (PDDA, Sigma Aldrich), 1% w/w, and 0.5 M NaCl, for 15 min. The substrates were carefully rinsed with bi-distilled water and then immersed into a GO solution (1 mg/mL) for 3 h. The final samples were rinsed with bi-distilled water and dried by a nitrogen stream. To perform the electrochemical reduction of GO, the bi-distilled water drop was placed on top of the samples and grounded by means of an external gold plate. The two interdigitated electrodes were short-circuited, and their potential was swept from 0 to −3 V until the expected grade of the GO reduction was achieved.

The fabricated rGO-TFTs have been characterized as water-gated transistors. Measurements were performed using bi-distilled water as gate medium and a platinum wire as gate electrode.

B. Ambipolar Transistors' Convention

Commonly used transistors are classified either as n-type transistors (charge carriers are electrons) or as p-type transistors (charge carriers are holes). In both the cases, the source and drain electrodes are easily identified without any ambiguity since only one type of charge carriers is involved in the charge transport; therefore, the source electrode is the electrode injecting the charges (either electrons or holes), and the drain electrode is the electrode where the charges are collected. In terms of applied potentials, in n-type transistors the source electrode is the one at lower potential, whereas in p-type transistors the source electrode is the one at higher potential (independently of the potential applied to the gate electrode).

Ambipolar transistors, however, can transport both electrons and holes, even simultaneously. Therefore, assigning a source or drain label to an electrode may be confusing. In fact, once applied a nonzero potential between these two electrodes, one electrode is the electron source and the hole drain; the opposite electrode is the electron drain and the hole source.

For sake of clarity, in this article, we moved away from what we may call the source and drain convention and we decided simply to label the two electrodes as negative (N) and positive (P). Contextually, we have chosen to apply only positive V_P potentials to the P electrode ($V_P \geq 0$ V), while only negative V_N potentials to the N electrode ($V_N \leq 0$ V). As a consequence, the I_{PN} current flowing from P to N is always positive; moreover, the N electrode is unambiguously the one that injects electrons (n-type source), while the P electrode is the one that injects holes (p-type source). Fig. 1(b) reports the conventions used in this work, whereas Table I summarizes the adopted terminology and abbreviations.

III. Results and Discussions

Our samples are fabricated over a silicon substrate, which is often used for the fabrication of bottom-gate bottom-contacts

TABLE I
AMBIPOLAR TRANSISTOR CONVENTIONS

Symbol	Definition	Notes and Description
G	Gate Electrode	
V_G	Gate Electrode Potential	It can assume either positive or negative values
BG	Bottom Gate Electrode	It is the n^{++}-Si substrate; only used for pre-characterization before adding the water drop
V_{BG}	Bottom-Gate Potential	Always 0 V during water-gated measurements
N	Negative Electrode	The **n-type** Source Electrode
V_N	Negative Electrode Potential	$V_N \leq 0$ V
V_{GN}	$V_G - V_N$	The **n-type** gate-to-source voltage
P	Positive Electrode	The **p-type** Source Electrode
V_P	Positive Electrode Potential	$V_P \geq 0$ V
V_{GP}	$V_G - V_P$	The **p-type** gate-to-source voltage
V_{PN}	$V_P - V_N$	$V_{PN} \geq 0$ V
I_{PN}	Current flowing from P to N	$I_{PN} \geq 0$ A

Abbreviations and Conventions used in this work.

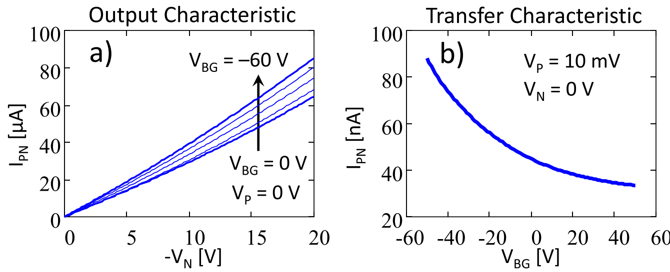

Fig. 2. (a) Bottom-gate output and (b) transfer characterization.

TFTs; therefore, we took advantage of the n^{++}-Si/SiO$_2$ substrate to test first our samples in a standard bottom-gate configuration (without the top-gate water drop). Fig. 2(a) reports the typical output characteristics recorded for different values of V_{BG}, and it shows that in this configuration, the samples mainly behave like a pristine resistance with a weak dependence on the applied V_{BG} potential. To emphasize the small bottom-gate field-effect behavior, we performed bottom-gate transfer characteristics for very low V_{PN} voltages ($V_N = 0$ V and $V_P = 10$ mV) while scanning V_{BG} from –50 up to +50 V. As shown in Fig. 2(b), the I_{PN} current monotonously decreases while scanning V_{BG} from negative to positive potentials, evidence of a p-type field-effect response. Moreover, the small current variation over 100 V V_{BG} scan confirms the always ON characteristic of these devices.

After bottom-gate characterizations, devices have been characterized as water-gated transistors. Using bi-distilled water as gate dielectric allows us a more efficient polarization of the rGO-based thin film due to a higher gate capacitance (i.e., SiO_2 versus H_2O: 17 nF/cm^2 versus 5 μF/cm^2 [5]). Moreover, according to the p-type behavior shown in Fig. 2, we decided to apply $V_N < 0$ V while keeping $V_P = 0$ V as reference ($V_P > V_N$), like it is normally done for p-type transistors. Fig. 3 reports the transfer curves of four different rGO-TFTs that differ from each other for the levels of reduction of the GO material (from sample A, highest reduction level, to sample D, lowest reduction level). Conversely to what is observed in Fig. 2(b), when the devices are polarized via bi-distilled water, the I_{PN} current features a well-defined parabolic shape that is characteristic of ambipolar transistors, allowing characterizing both the p-type and the n-type conductions. The pronounced hysteresis, particularly visible in sample D, is compatible with previous reports and it is typical of graphene- and rGO-based transistors [16].

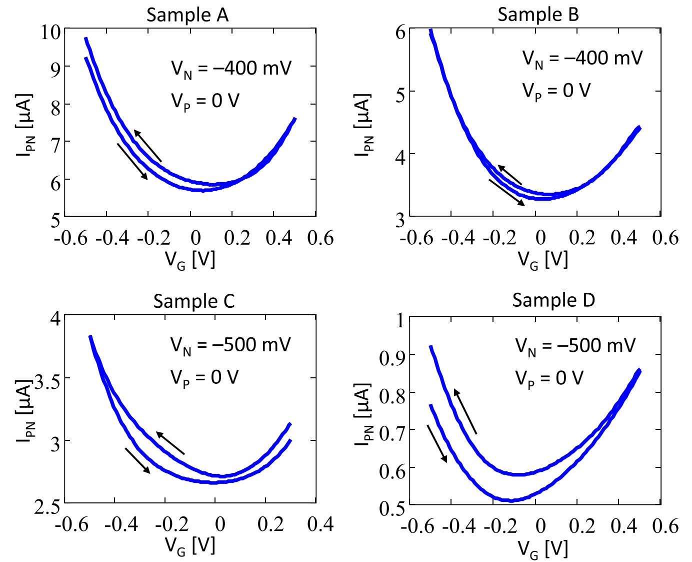

Fig. 3. Water-gate transfer characterization of four different samples ($V_{BG} = 0$ V during water-gated measurements).

Comparing the bottom- and water-gate characterizations, we can observe that despite the large difference between the bottom-gate capacitance (17 nF/cm^2) and the water-gate capacitance (5 μF/cm^2), the current magnitude recorded for $V_{PN} = 500$ mV stays in the order of few microamperes, suggesting that the characteristics of the devices are dominated by the rGO OFF-state conductivity during both bottom-gate and water-gate operation modes. However, the larger water-gate capacitance provides an effective field-effect modulation of the transistor current at very low voltages, whereas it is almost absent for bottom-gate voltages as large as 60 V.

Note that from the plots in Fig. 3, the p- and n-type currents roughly appear to have an equal contribution (quasi-symmetrical I_{PN} versus V_G curves); however, this symmetry originates from the choice of the applied voltages that emphasize the n-type part of the transistor: the largest applied n-type gate-to-source voltage ($V_{GN} = V_G - V_N = 1$ V) is two times larger than the largest p-type gate-to-source voltage ($V_{GP} = V_G - V_P = –500$ mV), promoting n-type conduction over the p-type conduction. Hence, rGO appears to be primarily a p-type semiconductor, but, to confirm this hypothesis, it is mandatory to apply a correct model for the estimation of the transistors mobilities and threshold voltages.

This investigation demands a clear understanding of the operation of this peculiar class of transistors. Although there are already several articles explaining the operative regions of ambipolar TFTs [17], we believe it is useful for the reader to report here a clear picture that summarizes how an ambipolar TFT goes from one region to the other while sweeping the

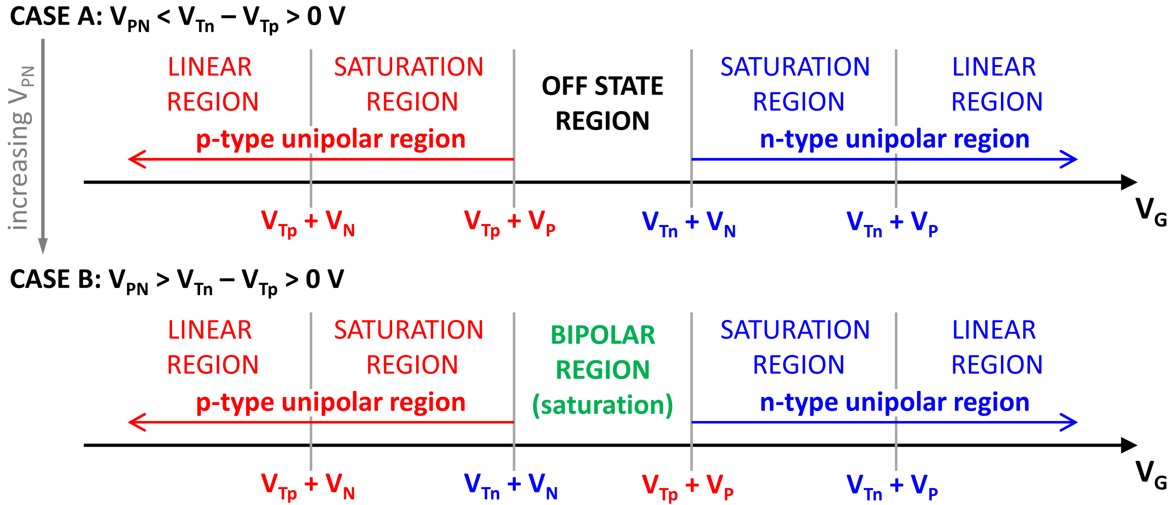

Fig. 4. Ambipolar TFT operating regions. Note that $V_{\mathrm{Tn}} > V_{\mathrm{Tp}}$.

gate voltage V_{G} (for fixed values of V_{N} and V_{P}), likewise during a transfer characterization. First, it is important to observe that ambipolar TFTs are characterized by two distinct threshold voltages, namely, V_{Tn} and V_{Tp} for n-type and p-type channels, respectively. Moreover, since electrons accumulate for positive overdrive voltages (V_{GN}–$V_{\mathrm{Tn}} > 0$ V) whereas holes accumulate for negative overdrive voltages (V_{GP}–$V_{\mathrm{Tp}} <$ 0 V), the condition $V_{\mathrm{Tn}} > V_{\mathrm{Tp}}$ must always be satisfied. Then, as sketched in Fig. 4, depending on the V_{PN} magnitude, two possible scenarios are plausible. When V_{PN} is lower than the threshold voltage difference V_{Tn}–V_{Tp}, the transistor can operate as a standard unipolar p-type transistor ($V_{\mathrm{G}} < V_{\mathrm{Tp}} + V_{\mathrm{P}}$), as a standard unipolar n-type transistor ($V_{\mathrm{G}} > V_{\mathrm{Tn}} + V_{\mathrm{N}}$), or it is in an OFF-state ($I_{\mathrm{PN_{FET}}} = 0$; $V_{\mathrm{Tp}} + V_{\mathrm{P}} < V_{\mathrm{G}} < V_{\mathrm{Tn}} + V_{\mathrm{N}}$). Conversely, when V_{PN} is larger than V_{Tn}–V_{Tp} the transistor can operate as a standard unipolar p-type transistor for $V_{\mathrm{G}} < V_{\mathrm{Tn}} + V_{\mathrm{N}}$, as standard unipolar n-type transistor for $V_{\mathrm{G}} > V_{\mathrm{Tp}} + V_{\mathrm{P}}$, or it operates in a bipolar regime ($V_{\mathrm{Tn}} + V_{\mathrm{N}} < V_{\mathrm{G}} < V_{\mathrm{Tp}} + V_{\mathrm{P}}$) in which electrons and holes are simultaneously injected from the N and P electrodes, respectively. In this last operating regime, carriers recombine inside the channel and the transistor is working as the series of a p-type transistor and an n-type transistor in the saturation regime [18].

Therefore, as depicted in Fig. 4, the gate-voltage dependent current in ambipolar TFTs is described by one of the five expressions reported in (1), as shown at the bottom of the page, as a function of the applied potentials. Where C_{i} is the water-gate capacitance, $\alpha_{p/n}$ is the mobility enhancement factor, and $\mu_{0p/n}$ is the carrier mobility when the overdrive voltage is equal to $V_{0p/n}$ (typically assumed as an empirical parameter). Therefore, the field-effect mobilities $\mu_{\mathrm{FET}p}$ and $\mu_{\mathrm{FET}n}$ can then be written as [19], [20]

$$\mu_{\mathrm{FET}p} = \mu_{0p}\left(\frac{V_{\mathrm{G}} - V_{\mathrm{Tp}} - V_{\mathrm{P}}}{V_{0p}}\right)^{\alpha_p} \tag{2}$$

$$\mu_{\mathrm{FET}n} = \mu_{0n}\left(\frac{V_{\mathrm{G}} - V_{\mathrm{Tn}} - V_{\mathrm{N}}}{V_{0n}}\right)^{\alpha_n}. \tag{3}$$

Note that (1)–(3) are typically used to model the current in disordered organic TFTs [21]. However, because rGO is rich in defect-induced localized mid-gap states that give rise to hopping transport mechanisms [22], their validity can also be extended for rGO-TFTs.

In addition to the field-effect behavior described in (1), the always-ON behavior observed in Fig. 2 confirms the presence of an OFF-state current contribution, mostly independent of the gate voltage V_{G}. Then, the recorded I_{PN} current can be written as a sum of $I_{\mathrm{PN_{FET}}}$ [see (1)] plus a constant OFF-current that we model by introducing a constant resistance R_{PN} in parallel with the transistor, thus describing the OFF-state conductivity

$$I_{\mathrm{PN_{FET}}} = \frac{W}{L}C_i \cdot \begin{cases} \dfrac{\mu_{0p}}{2+\alpha_p}\left[\left(\dfrac{V_{\mathrm{G}} - V_{\mathrm{Tp}} - V_{\mathrm{P}}}{V_{0p}}\right)^{2+\alpha_p} - \left(\dfrac{V_{\mathrm{G}} - V_{\mathrm{Tp}} - V_{\mathrm{N}}}{V_{0p}}\right)^{2+\alpha_p}\right] & \text{Linear (type P)} \\ \dfrac{\mu_{0p}}{2+\alpha_p}\left(\dfrac{V_{\mathrm{G}} - V_{\mathrm{Tp}} - V_{\mathrm{P}}}{V_{0p}}\right)^{2+\alpha_p} & \text{Saturation (type P)} \\ \left[\dfrac{\mu_{0p}}{2+\alpha_p}\left(\dfrac{V_{\mathrm{G}} - V_{\mathrm{Tp}} - V_{\mathrm{P}}}{V_{0p}}\right)^{2+\alpha_p} + \dfrac{\mu_{0n}}{2+\alpha_n}\left(\dfrac{V_{\mathrm{G}} - V_{\mathrm{Tn}} - V_{\mathrm{N}}}{V_{0n}}\right)^{2+\alpha_n}\right] & \text{Bipolar} \\ \dfrac{\mu_{0n}}{2+\alpha_n}\left(\dfrac{V_{\mathrm{G}} - V_{\mathrm{Tn}} - V_{\mathrm{N}}}{V_{0n}}\right)^{2+\alpha_n} & \text{Saturation (type N)} \\ \dfrac{\mu_{0n}}{2+\alpha_n}\left[\left(\dfrac{V_{\mathrm{G}} - V_{\mathrm{Tn}} - V_{\mathrm{N}}}{V_{0n}}\right)^{2+\alpha_n} - \left(\dfrac{V_{\mathrm{G}} - V_{\mathrm{Tn}} - V_{\mathrm{P}}}{V_{0n}}\right)^{2+\alpha_n}\right] & \text{Linear (type N)} \end{cases} \tag{1}$$

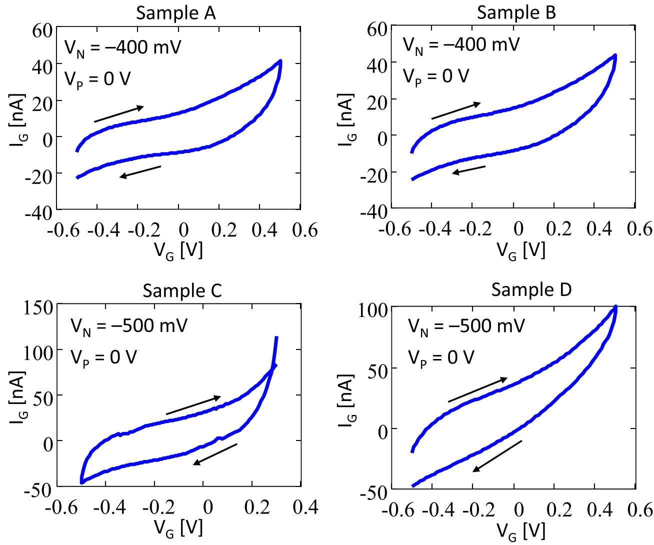

Fig. 5. Water-gate leakage current recorded during the transfer characteristics reported in Fig. 3.

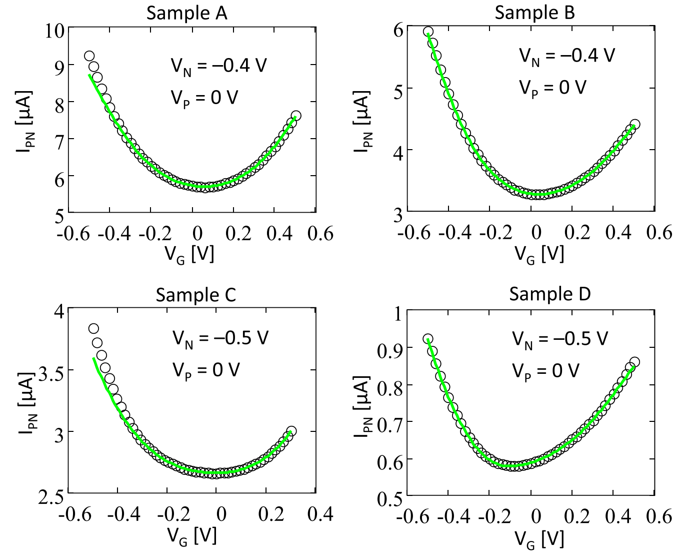

Fig. 6. Fitting of the data in Fig. 3 using the equations described in this article (black circles are the experimental data, whereas the green solid lines are the fitting curves).

of the device

$$I_{\mathrm{PN}} = I_{\mathrm{PN_{FET}}} + \frac{V_{\mathrm{P}} - V_{\mathrm{N}}}{R_{\mathrm{PN}}}. \tag{4}$$

In the proposed model, we neglect the possible presence of charge-transfer phenomena occurring at the interface between water and rGO film. In fact, the voltages applied during characterization of our devices have been chosen sufficiently low to avoid the triggering of water splitting and redox processes. To confirm that, we monitored the leakage current I_{G} during the recording of devices' transfer characteristics. As shown in Fig. 5, the leakage current is much lower than the I_{PN} current, and hence, it can be considered negligible; moreover, the leakage current during the forward and reverse V_{G} scan exhibits mainly a capacitive behavior without any evidence of oxidation or reduction peaks (for a comprehensive reference, the reader may refer to [23]). Therefore, any parasitic charge transfer phenomena, if present, is negligible and we can safely apply the presented model to our devices.

Fig. 6 shows the excellent agreement between the data and the model that is capable of fully describing the operation of the devices in all their operative regions and it allows for a good estimation of the rGO-TFTs parameters and of the OFF-state conductivity. The transistor parameters, summarized in Table II, were extrapolated by applying the method reported in [24] to both the p- and n-type branches while using R_{PN} as a fitting parameter. To compare the p- and n-type behaviors of the TFTs, the field-effect mobilities $\mu_{\mathrm{FET}p}$ and $\mu_{\mathrm{FET}n}$ were evaluated for the same overdrive voltage $|V_{\mathrm{GP}}–V_{\mathrm{Tp}}| = |V_{\mathrm{GN}}–V_{\mathrm{Tn}}| = 0.5$ V.

Notably, the carrier mobility increases with the reduction level of GO confirming that the electrochemical reduction is partially restoring the aromatic structure of graphene increasing the number of conductive states for electrons and holes. Conversely, the mobility enhancement factors α_p and α_n do not display any particular trend. The parameter $\alpha_{p/n}$ is typically representative of the material disorder. In principle, lower $\alpha_{p/n}$ should be expected for higher mobilities. However, the value of

TABLE II
FITTING PARAMETERS

Sample	R_{PN} [kΩ]	μ_{FET_p} [a] [$cm^2V^{-1}s^{-1}$]	μ_{FET_n} [a] [$cm^2V^{-1}s^{-1}$]	V_{Tp} [V]	V_{Tn} [V]	α_p	α_n	σ^2 [b] [$\cdot 10^{-5}$]
A	70	$7.2\cdot10^{-3}$	$7.3\cdot10^{-3}$	0.11	0.42	0.55	0.43	17.1
B	122	$7\cdot10^{-3}$	$3.7\cdot10^{-3}$	0.08	0.42	0.68	0.03	0.7
C	188	$2.9\cdot10^{-3}$	$3.9\cdot10^{-3}$	0.05	0.46	0.94	0.79	27.4
D	864	$1.7\cdot10^{-3}$	$0.5\cdot10^{-3}$	–0.11	0.38	0.08	0.08	1.44

Computed fitting parameters used in Fig. 5

[a] μ_{FET_p} and μ_{FET_n} are computed for the same overdrive voltage $|V_{GP} - V_{Tp}| = |V_{GN} - V_{Tn}| = 0.5\,V$.

[b] Standard deviation σ^2 is used to report the goodness of the fit.

$\alpha_{p/n}$ can be related to different factors worthy of investigation. These include: 1) the die-to-die variation in the quality of the GO layer before the reduction process; 2) the presence of hysteresis during transfer characterizations that can introduce a small degree of uncertainty on the extrapolated parameters; and 3) the ratio between the number of new conductive states and defects during reduction (on one hand, electrochemical reduction increases the number of conductive states; on the other hand, it also increases the material disorder). Remarkably, the estimated values of α_p and α_n are between 0 and 1, indicating a relatively low degree of disorder comparable to other organic and inorganic thin-film materials [25], [26].

As reported in Table II, there is not a relevant difference between the two mobilities that can be roughly considered the same for electrons and holes. Therefore, rGO-TFTs are capable of equally transporting holes and electrons. The predominance in the transfer characteristics of the p-type branch over the n-type branch is not given by a larger hole mobility, but it derives from the imbalance between the two threshold voltages. In fact, if we define a mean threshold voltage as $V_{\mathrm{Tm}} = (V_{\mathrm{Tp}} + V_{\mathrm{Tn}})/2$, we find a value around +250 mV, where positive sign indicates that lower gate voltages are needed to form the p-channel than the n-channel, explaining the predominance of the observe p-type behavior. It is important to remark that the reported value of V_{Tm} is not an

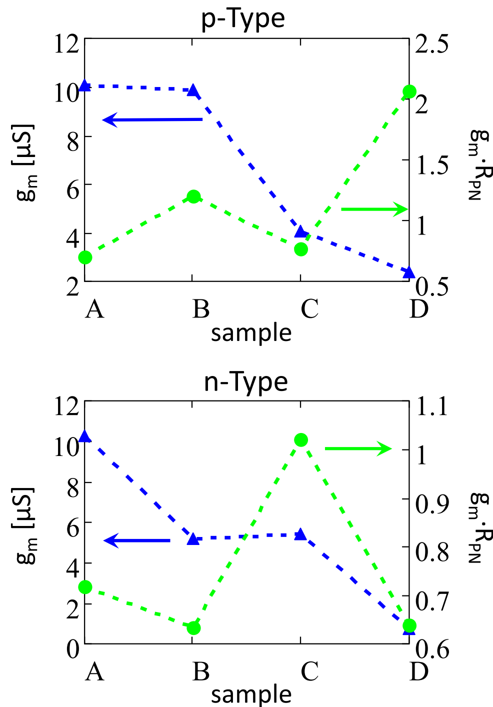

Fig. 7. Transconductances g_m for different samples (blue triangles). The g_m values were calculated using the data reported in Table II and were computed for the same overdrive voltage $|V_{GP} - V_{Tp}| = |V_{GN} - V_{Tn}| = 0.5$ V. The green circles in the figure represent the corresponding $g_m \cdot R_{PN}$ product.

intrinsic property of the rGO layer, but it is in large extent determined by several contributions, alike a conventional MOS structure [27]: the alignment between the Fermi energy of rGO; the work function of the gate electrode; the state at the rGO/electrolyte interface; the bulk oxide trapped charge at the bottom gate; and the interface states at the bottom gate.

IV. Feasibility of rGO-Based Transistors and Circuits

From the application point of view, a final consideration is worth to be done. A key parameter used during the design of transistor-based analog applications is the transconductance g_m. The higher its value, the higher the potentiality of the transistor to amplify an input signal; however, this reasoning is true only when the in-parallel parasitic conductance $((1/R_{PN}))$ is negligible compared with the magnitude of g_m (i.e., $g_m \gg (1/R_{PN})$). It is easy to show that if $g_m \cdot R_{PN} < 1$, the design of even the most basic voltage amplifier (e.g., a cascode voltage amplifier) becomes impossible. As plotted in Fig. 6, g_m increases by increasing the reduction level of GO, but at the same time R_{PN} decreases. This highlights the impact of the reduction process on the rGO-TFTs performance: on one hand, it increases TFTs' performance giving rise to higher g_m; on the other hand, it reduces the energy gap of GO leading to a semimetallic behavior that lowers the value of R_{PN}.

The development of a suitable and optimized reduction technique for GO is out of the scope of this article. However, the data in Fig. 7 show that even though in most cases the product $g_m \cdot R_{PN}$ is smaller than one, in some cases it is possible to also obtain $g_m \cdot R_{PN} > 1$. This is why it is fundamental to improve the reduction technique of GO to fully benefit from the electronic properties of graphene derivatives and fabricate TFTs with high transconductances while keeping the OFF-state conductivity limited.

V. Conclusion

In this work, we analyzed the electrical characteristics of ambipolar rGO-TFTs, modeling their behavior and including an in-parallel resistance to describe the OFF-state conductivity of the devices. The extracted parameters give us an insight into the conduction mechanism of rGO-based transistors, allowing us to investigate the unbalance between p- and n-type conductions. The p-type predominance of the tested rGO-TFTs is not due to a larger p-type field-effect mobility but it originates from a positive shift on the threshold voltages.

We stressed the fundamental importance of the OFF-state conductivity of rGO-based TFTs that must be carefully taken into account for correct estimation of the device parameters. To the best of our knowledge, this aspect has always been neglected in previously reported data, and it should be diligently evaluated in all the future studies.

Furthermore, the electronic behavior of rGO-TFTs is largely dominated by its large OFF-state current that we should critically ask ourselves: "Is it correct to call this class of devices transistors? Or, should we just treat them as variable resistors?"

We believe that this question will fuel a new batch of experiments to achieve deeper knowledge on this class of devices. Such a challenge aims to overcome the present limits of rGO technology using alternative methods for GO deposition and reduction and to examine original TFT architectures.

References

[1] "15 years of graphene electronics," *Nat. Electron.*, vol. 2, no. 9, p. 369, Sep. 2019, doi: 10.1038/s41928-019-0312-4.

[2] J.-H. Chen, C. Jang, S. Xiao, M. Ishigami, and M. S. Fuhrer, "Intrinsic and extrinsic performance limits of graphene devices on SiO_2," *Nature Nanotechnol.*, vol. 3, no. 4, pp. 206–209, Mar. 2008, doi: 10.1038/nnano.2008.58.

[3] C. Gómez-Navarro *et al.*, "Electronic transport properties of individual chemically reduced graphene oxide sheets," *Nano Lett.*, vol. 7, no. 11, pp. 3499–3503, Nov. 2007, doi: 10.1021/nl072090c.

[4] Q. He *et al.*, "Transparent, flexible, all-reduced graphene oxide thin film transistors," *ACS Nano*, vol. 5, no. 6, pp. 5038–5044, Jun. 2011, doi: 10.1021/nn201118c.

[5] R. Furlan de Oliveira *et al.*, "Liquid-gated transistors based on reduced graphene oxide for flexible and wearable electronics," *Adv. Funct. Mater.*, vol. 29, no. 46, Nov. 2019, Art. no. 1905375, doi: 10.1002/adfm.201905375.

[6] P. Lin and F. Yan, "Organic thin-film transistors for chemical and biological sensing," *Adv. Mater.*, vol. 24, no. 1, pp. 34–51, Jan. 2012, doi: 10.1002/ADMA.201103334.

[7] N. Lago and A. Cester, "Flexible and organic neural interfaces: A review," *Appl. Sci.*, vol. 7, no. 12, p. 1292, Dec. 2017, doi: 10.3390/app7121292.

[8] T. Cramer *et al.*, "Organic ultra-thin film transistors with a liquid gate for extracellular stimulation and recording of electric activity of stem cell-derived neuronal networks," *Phys. Chem. Chem. Phys.*, vol. 15, no. 11, pp. 3897–3905, Mar. 2013, doi: 10.1039/c3cp44251a.

[9] B. M. Blaschke *et al.*, "Flexible graphene transistors for recording cell action potentials," *2D Mater.*, vol. 3, no. 2, Apr. 2016, Art. no. 025007, doi: 10.1088/2053-1583/3/2/025007.

[10] N. Lago *et al.*, "TIPS-pentacene as biocompatible material for solution processed high-performance electronics operating in water," *IEEE Electron Device Lett.*, vol. 39, no. 9, pp. 1401–1404, Sep. 2018, doi: 10.1109/LED.2018.2856462.

[11] I. Meric, M. Y. Han, A. F. Young, B. Ozyilmaz, P. Kim, and K. L. Shepard, "Current saturation in zero-bandgap, top-gated graphene field-effect transistors," *Nature Nanotechnol.*, vol. 3, no. 11, pp. 654–659, Sep. 2008, doi: 10.1038/nnano.2008.268.

[12] D. Kireev *et al.*, "Graphene transistors for interfacing with cells: Towards a deeper understanding of liquid gating and sensitivity," *Sci. Rep.*, vol. 7, no. 1, pp. 1–12, Jul. 2017, doi: 10.1038/s41598-017-06906-5.

[13] F. A. D. Santos, N. C. S. Vieira, N. A. Zambianco, B. C. Janegitz, and V. Zucolotto, "The layer-by-layer assembly of reduced graphene oxide films and their application as solution-gated field-effect transistors," *Appl. Surf. Sci.*, vol. 543, Mar. 2021, Art. no. 148698, doi: 10.1016/j.apsusc.2020.148698.

[14] S. Vasilijević, G. Mattana, G. Anquetin, N. Battaglini, and B. Piro, "Electrochemical tuning of reduced graphene oxide in printed electrolyte-gated transistors. Impact on charge transport properties," *Electrochimica Acta*, vol. 371, Mar. 2021, Art. no. 137819, doi: 10.1016/j.electacta.2021.137819.

[15] E. Piccinini, C. Bliem, C. Reiner-Rozman, F. Battaglini, O. Azzaroni, and W. Knoll, "Enzyme-polyelectrolyte multilayer assemblies on reduced graphene oxide field-effect transistors for biosensing applications," *Biosensors Bioelectron.*, vol. 92, pp. 661–667, Jun. 2017, doi: 10.1016/j.bios.2016.10.035.

[16] H. Wang, Y. Wu, C. Cong, J. Shang, and T. Yu, "Hysteresis of electronic transport in graphene transistors," *ACS Nano*, vol. 4, no. 12, pp. 7221–7228, Dec. 2010, doi: 10.1021/nn101950n.

[17] Y. Ren, X. Yang, L. Zhou, J. Mao, S. Han, and Y. Zhou, "Recent advances in ambipolar transistors for functional applications," *Adv. Funct. Mater.*, vol. 29, no. 40, Oct. 2019, Art. no. 1902105, doi: 10.1002/ADFM.201902105.

[18] A. Risteska and D. Knipp, "Organic ambipolar transistors and circuits," in *Handbook of Visual Display Technology*. Cham, Switzerland: Springer, Jan. 2016, pp. 971–995, doi: 10.1007/978-3-319-14346-0_177.

[19] P. V. Necliudov, M. S. Shur, D. J. Gundlach, and T. N. Jackson, "Modeling of organic thin film transistors of different designs," *J. Appl. Phys.*, vol. 88, no. 11, p. 6594, Nov. 2000, doi: 10.1063/1.1323534.

[20] G. Horowitz, M. E. Hajlaoui, and R. Hajlaoui, "Temperature and gate voltage dependence of hole mobility in polycrystalline oligothiophene thin film transistors," *J. Appl. Phys.*, vol. 87, no. 9, pp. 4456–4463, Apr. 2000, doi: 10.1063/1.373091.

[21] O. Marinov, M. J. Deen, U. Zschieschang, and H. Klauk, "Organic thin-film transistors: Part I—Compact DC modeling," *IEEE Trans. Electron Devices*, vol. 56, no. 12, pp. 2952–2961, Dec. 2009, doi: 10.1109/TED.2009.2033308.

[22] P. Sehrawat, S. S. Islam, P. Mishra, and S. Ahmad, "Reduced graphene oxide (rGO) based wideband optical sensor and the role of temperature, defect states and quantum efficiency," *Sci. Rep.*, vol. 8, no. 1, pp. 1–13, Dec. 2018, doi: 10.1038/s41598-018-21686-2.

[23] A. J. Bard and L. R. Faulkner, *Electrochemical Methods: Fundamentals and Applications*, 2nd ed. Hoboken, NJ, USA: Wiley, 2001.

[24] P. Servati, D. Striakhilev, and A. Nathan, "Above-threshold parameter extraction and modeling for amorphous silicon thin-film transistors," *IEEE Trans. Electron Devices*, vol. 50, no. 11, pp. 2227–2235, Nov. 2003, doi: 10.1109/TED.2003.818156.

[25] M. Buonomo *et al.*, "Simple and accurate single transistor technique for parameters extraction from organic and inorganic thin film devices," *Organic Electron.*, vol. 63, pp. 376–383, Dec. 2018, doi: 10.1016/j.orgel.2018.08.008.

[26] N. Lago *et al.*, "Investigation of mobility transient on organic transistor by means of DLTS technique," *IEEE Trans. Electron Devices*, vol. 63, no. 11, pp. 4432–4439, Nov. 2016, doi: 10.1109/TED.2016.2611142.

[27] S. M. Sze and M.-K. Lee, *Semiconductor Devices: Physics and Technology*, 3rd ed. Hoboken, NJ, USA: Wiley, 2012.

Open Access funding provided by 'Università degli Studi di Padova' within the CRUI-CARE Agreement